Length dependence of ionization potentials of transacetylenes: Internally consistent DFT/*GW* approach

Max Pinheiro Jr. and Marilia J. Caldas
Instituto de Física, Universidade de São Paulo, Caixa Postal 66318, CEP 05315-970 São Paulo SP, Brazil

Patrick Rinke
COMP Centre of Excellence and Helsinki Institute of Physics, Department of Applied Physics, Aalto University, P.O. Box 11100, FI-00076 Aalto, Espoo, Finland and Fritz-Haber-Institut der Max-Planck-Gesellschaft, Berlin D-14195, Germany

Volker Blum
Department of Mechanical Engineering and Materials Science and Center for Materials Genomics, Duke University, Durham, North Carolina 27708, USA and Fritz-Haber-Institut der Max-Planck-Gesellschaft, Berlin D-14195, Germany

Matthias Scheffler
Fritz-Haber-Institut der Max-Planck-Gesellschaft, Berlin D-14195, Germany

(Received 26 February 2015; published 18 November 2015)

We follow the evolution of the ionization potential (IP) for the paradigmatic quasi-one-dimensional transacetylene family of conjugated molecules, from short to long oligomers and to the infinite polymer transpolyacetylene (TPA). Our results for short oligomers are very close to experimental available data. We find that the IP varies with oligomer length and converges to the given value for TPA with a smooth, coupled inverse-length-exponential behavior. Our prediction is based on an "internally consistent" scheme to adjust the exchange mixing parameter α of the PBEh hybrid density functional, so as to obtain a description of the electronic structure consistent with the quasiparticle approximation for the IP. This is achieved by demanding that the corresponding quasiparticle correction, in the GW@PBEh approximation, vanishes for the IP when evaluated at PBEh(α^{ic}). We find that α^{ic} is also system-dependent and converges with increasing oligomer length, enabling the dependence of the IP and other electronic properties to be identified.

DOI: 10.1103/PhysRevB.92.195134 PACS number(s): 31.15.A−, 36.20.Kd, 32.10.Hq, 31.15.xm

I. INTRODUCTION

Ionization potentials (IPs) and electron affinities (EAs) are fundamental electronic properties of composite or complex systems. In recent years, when organic materials (molecular or polymeric) have been sought for applications in optoelectronic devices [1,2], much attention has been paid to this subject. The input from theoretical calculations is extremely relevant not only to help evaluate experimental data, but also to identify new directions for the optimal composition of actors in the building of a device. There has thus been a search for theoretical methods that can give us accuracy together with feasibility of calculations, spanning a wide range of both inorganic and organic molecular systems [3–6]. In particular, the class of linear or quasilinear molecular systems—oligomers or polymers—offers a special work space that allows one to concentrate on the length dependence (just one relevant dimension) of the properties of interest: indeed, the dependence and evolution of the IP, the EA, and the electronic gaps with structural characteristics or compositions is a topic of intense study [7–12]. For short oligomers in fixed geometries, as for small molecules, these properties can be obtained with high accuracy from high-level quantum-chemistry calculations that go beyond the mean-field approximation, serving as benchmarks for other computational electronic structure approaches [13,14]. As the oligomer length increases, however, the computational cost of such calculations quickly becomes prohibitive [15].

For such polyatomic systems, in particular for large molecules or extended materials, density-functional theory (DFT) has become the method of choice for a theoretical description, analysis, or prediction of ground-state electronic properties, stable or metastable atomic structures, vibrations, and structure-property relationships [12,16,17]. We recall that, despite the fact that DFT is a ground-state theory, certain excitations that can be expressed as differences of ground-state total energies are accessible. The IP and the EA are defined as

$$\mathrm{IP} = E^{N-1} - E^{N}, \tag{1}$$

$$\mathrm{EA} = E^{N} - E^{N+1}, \tag{2}$$

where E^N, E^{N-1}, and E^{N+1} are the total energies of the N-, $(N-1)$-, and $(N+1)$-particle systems in the ground state. If E^N and $E^{N\pm1}$ are computed for the same molecular geometry, we obtain "vertical excitations." The difference

$$E_{\mathrm{gap}} = \mathrm{IP} - \mathrm{EA} \tag{3}$$

is the electronic gap of the system, also called the self-consistent or ΔSCF gap. Experimentally it is determined by direct and inverse photoemission, and it should not be taken as the optical gap.

In exact DFT, the values of the IP and the EA from Eqs. (1) and (2) are also given [18,19] by the highest occupied Kohn-Sham (KS) levels of the N- and $(N+1)$-electron systems,

respectively. For approximate DFT, the Slater-Janak transition states, i.e., the highest occupied KS levels of the $(N-1/2)$- and of the $(N+1/2)$-electron systems, should provide an accurate estimate of the IP and EA energies:

$$\mathrm{IP} \approx \epsilon_N^{N-1/2}, \tag{4}$$

$$\mathrm{EA} \approx \epsilon_{N+1}^{N+1/2}. \tag{5}$$

The difference between the highest occupied KS levels of the N- and $(N-1/2)$- and of the $(N+1/2)$- and $(N+1)$-electron systems reflects the self-interaction or localization error of the highest occupied KS orbitals of the N and $(N+1)$-electron systems [20]. For approximate DFT, the energies noted in Eqs. (4) and (5) should be taken [21,22].

The HOMO and LUMO (highest occupied and lowest unoccupied molecular orbital) levels of KS theory for the ground-state of a given N-electron system, that is, the ϵ_N^N and ϵ_{N+1}^N energies, are, however, frequently used for the definitions of (the negative of) IP and EA, and the difference

$$E_{\mathrm{gap}}^{\mathrm{KS}} = \epsilon_{N+1}^N - \epsilon_N^N \tag{6}$$

is usually termed the Kohn-Sham HOMO-LUMO gap.

As was mentioned above, the use of beyond-mean-field methods for large systems is still a challenging issue, and for this reason it is not known how the IP or the electronic gap develop as a function of polymer length. While Berger *et al.* showed [23], through a "dielectric needle" model for the polymer, that the polarizability per monomer unit is inversely proportional to the polymer length, no such analytic dependence is known for the ionization potential. For approximate DFT functionals, the IP from Eq. (1), $\mathrm{IP}_{\Delta\mathrm{SCF}}$, is usually more accurate than that from the plain HOMO energy $-\epsilon_N^N$ because it is less affected by the self-interaction error [24]. However, going from short oligomers to more extended systems, different DFT functionals give rise to a different length dependence of the $\mathrm{IP}_{\Delta\mathrm{SCF}}$, ranging from concave and straight to convex as a function of inverse length [25], so the problem is still under discussion.

To address this problem, we will design a DFT functional consistent with many-body perturbation theory in the GW approach [26,27]. GW has become the prime method for the computation of quasiparticle energies in solids as measured by direct or inverse photoemission [28–30] and is increasingly applied to organic systems [31,32] including polymers [15,33–39]. The standard procedure is to apply a single iteration of the GW approach (G_0W_0) as a many-body perturbation to the results of a DFT or Hartree-Fock (HF) calculation. The single-particle wave functions of DFT or HF, the respective orbital energies, and the resulting dielectric screening form the input to the G_0W_0 calculation and therefore determine the behavior of the screened Coulomb interaction W_0. The screening strength of W decreases with an increase of the HOMO-LUMO gap. Thus local or semilocal DFT functionals that produce a too small gap compared to the real electronic gap would overestimate screening, whereas HF that produces a too large gap would underestimate it. As shown recently by Bruneval and Marques [40], input orbitals and energies derived from hybrid functionals with a high fraction of exact-exchange yield G_0W_0 IPs that agree well with experiment for small organic molecules, whereas for larger molecules the fraction of exact exchange has to be considerably lower [41–43]. In other words, there is a well-known *starting-point dependence* of the G_0W_0 approach [43–45], and the best DFT starting point is usually also system-dependent. It would therefore be desirable to iterate the GW approach toward self-consistency to eliminate the starting point dependence. Different schemes have been developed, either achieving self-consistency directly [46,47] or by the so-called "quasiparticle self-consistency" of Schilfgaarde *et al.* [48], which determines the variationally best noninteracting Green's function G_0. The present work will follow a simpler and numerically more efficient approach.

We apply here the G_0W_0@DFT approach to quasilinear systems of increasing length. Transpolyacetylene—$(C_2H_2)_n$—is the simplest conjugated material that already exhibits the alternating set of sp^2-bonded carbon atoms, common to all conducting polymers, which leads to π-delocalization of the frontier molecular orbitals dictating the behavior of the electronic gap [49]. We will thus use the transacetylene (TA) family, from small oligomers (OTAs) to the infinite polymer (TPA), as a model system to investigate the dependence of basic properties such as the IP and the HOMO-LUMO gap with localization length. To do that, we follow an approach [50,51] proposed recently: Building on the fact that the Kohn-Sham energy ϵ_N of the HOMO gives us the IP in exact DFT, we vary the amount of exact exchange in the Perdew-Burke-Ernzerhof hybrid functional [52,53] (PBEh). We then pick that admixture α of exact exchange for which the KS-HOMO eigenvalue agrees with the quasiparticle energy from a G_0W_0 calculation based on the same PBEh(α) starting point, denoted G_0W_0@PBEh(α^{ic}). The HOMO of PBEh is now consistent with the quasiparticle removal energy of G_0W_0, and for this reason we call our scheme internally consistent ic-PBEh. Monitoring α^{ic} for oligomers with increasing length then allows us to assess the length dependence of the IP and to gather information on the electronic screening.

The remainder of the paper is organized as follows: In Sec. II, we provide a short overview of the basic concepts of the G_0W_0 approximation and some technical aspects of the implementation. In Sec. III, we present our results, starting from the ground-state DFT calculations, to obtain the geometrical models for the oligomers; we next present and discuss the internally consistent model, applied to study the ionization potential of TA oligomers, with a special focus on the length dependence. Finally, we draw our conclusions in Sec. IV.

II. THEORETICAL BACKGROUND

In many-body perturbation theory, the single-particle excitation energies are the solutions of the quasiparticle equation,

$$\left[-\frac{\nabla^2}{2}+v_{\mathrm{ext}}(\mathbf{r})+v_H(\mathbf{r})\right]\psi_{n\sigma}(\mathbf{r})+\int d\mathbf{r}'\,\Sigma_\sigma\left(\mathbf{r},\mathbf{r}';\epsilon_{n\sigma}^{\mathrm{qp}}\right)\psi_{n\sigma}(\mathbf{r}') = \epsilon_{n\sigma}^{\mathrm{qp}}\psi_{n\sigma}(\mathbf{r}), \tag{7}$$

where v_{ext} corresponds to the external potential created by the nuclei, v_H is the Hartree potential, n is a state index, and σ is the associated spin. The nonlocal complex self-energy operator Σ contains all electron-electron interaction effects beyond the Hartree mean field. In practice the self-energy needs to be approximated, and here we adopt Hedin's GW approximation

[26,54] at the one-shot level,

$$\Sigma_\sigma^{GW}(\mathbf{r},\mathbf{r}',\epsilon) = \frac{i}{2\pi}\int d\epsilon' G_0^\sigma(\mathbf{r},\mathbf{r}',\epsilon+\epsilon')W_0(\mathbf{r},\mathbf{r}',\epsilon')e^{i\epsilon\eta}, \tag{8}$$

where η is an infinitesimal positive number. W_0 is the screened Coulomb interaction,

$$W_0(\mathbf{r},\mathbf{r}',\epsilon) = \int d\mathbf{r}''\varepsilon^{-1}(\mathbf{r},\mathbf{r}'',\epsilon)v(\mathbf{r}''-\mathbf{r}'), \tag{9}$$

where $v(\mathbf{r}-\mathbf{r}') = 1/|\mathbf{r}-\mathbf{r}'|$ is the bare Coulomb interaction and $\varepsilon^{-1}(\mathbf{r},\mathbf{r}'';\epsilon)$ is the inverse dielectric function. The latter can be written in terms of the polarizability

$$\varepsilon(\mathbf{r},\mathbf{r}',\epsilon) = \delta(\mathbf{r}-\mathbf{r}') - \int d\mathbf{r}'' v(\mathbf{r}-\mathbf{r}'')P_0(\mathbf{r}'',\mathbf{r}';\epsilon) \tag{10}$$

with

$$P_0(\mathbf{r},\mathbf{r}';\epsilon) = -\frac{i}{2\pi}\sum_\sigma\int d\epsilon' e^{i\epsilon'\eta}G_0^\sigma(\mathbf{r},\mathbf{r}';\epsilon+\epsilon')G_0^\sigma(\mathbf{r}',\mathbf{r};\epsilon'). \tag{11}$$

Finally, G_0 is calculated from the eigenenergies and wave functions of a preceding DFT or HF calculation,

$$G_0^\sigma(\mathbf{r},\mathbf{r}';\epsilon) = \sum_n \frac{\psi_{n\sigma}(\mathbf{r})\psi_{n\sigma}^*(\mathbf{r}')}{\epsilon-[\epsilon_{n\sigma}+i\eta\ \mathrm{sgn}(\epsilon_F-\epsilon_{n\sigma})]}. \tag{12}$$

Making the additional approximation that the quasiparticle wave functions equal the Kohn-Sham states, we can simplify Eq. (7) and write for the real part of the quasiparticle energies

$$\epsilon_{n\sigma}^{\mathrm{qp}} = \epsilon_{n\sigma}^{\mathrm{KS}} + \mathrm{Re}\langle\psi_{n\sigma}|\Sigma_\sigma^{GW}\left(\epsilon_{n\sigma}^{\mathrm{qp}}\right) - v_{\mathrm{xc}}|\psi_{n\sigma}\rangle = \epsilon_{n\sigma}^{\mathrm{KS}} + \Delta_{n\sigma}^{\mathrm{qp}}, \tag{13}$$

where v_{xc} is the exchange-correlation potential of the underlying DFT (or HF) calculation, and $\Delta_{n\sigma}^{\mathrm{qp}} = \mathrm{Re}\langle\psi_{n\sigma}|\Sigma^{GW}(\epsilon_{n\sigma}^{\mathrm{qp}}) - v_{\mathrm{xc}}|\psi_{n\sigma}\rangle$ is the G_0W_0 or quasiparticle correction. Equations (8)–(13) illustrate that $\Delta_{n\sigma}^{\mathrm{qp}}$ and therefore the quasiparticle energies depend on the DFT functional used in the preceding calculation.

As stated in the Introduction, in exact DFT the HOMO level of a finite system gives the IP, and therefore the self-energy correction $\Delta_{\mathrm{HOMO}}^{\mathrm{qp}}$ is zero (for any other level, no such statement holds). In standard approximations to the exchange-correlation functional, the IP is typically not given accurately because of the self-interaction error. Minimizing the absolute value of $\Delta_{\mathrm{HOMO}}^{\mathrm{qp}}$ through optimization of α therefore implies that the self-energy correction to the HOMO level should be as small as possible. Alternatively, we could stay entirely within DFT and enforce the linearity of the DFT total energy with respect to the occupation of the HOMO state [24] to obtain α. However, this is beyond the scope of this paper, and we will defer a discussion of the deviation of the straight line behavior and the internally consistent GW scheme to a forthcoming paper.

We emphasize that α is not related to a shift of the chemical potential (ϵ_s) that was originally proposed by Hedin [26], who observed that if introduced in G_0W_0 calculations it would model some effects of fully self-consistent GW calculations. The shift ϵ_s is also implemented in the GW space-time code [55] and has negligible effects on the quasiparticle energies of semiconductors and insulators. This observation by Rieger *et al.* [55] is in line with the findings by Pollehn *et al.* [56], who observe differences between G_0W_0, shifted G_0W_0, and self-consistent GW only in the satellite spectrum of their Hubbard clusters and not in the quasiparticle peaks.

To summarize this section, in the internally consistent GW scheme we explore the space of possible G_0 starting points spanned by the PBEh hybrid functional, and we use the α parameter to traverse this space. In practice, we start from the same hybrid functional [52] model of Perdew, Ernzerhof, and Burke,

$$E_{\mathrm{xc}} = \alpha E_x^{\mathrm{EX}} + (1-\alpha)E_x^{\mathrm{PBE}} + E_c^{\mathrm{PBE}}, \quad 0 \leqslant \alpha \leqslant 1, \tag{14}$$

where E^{EX} denotes the exact-exchange energy, and E_x^{PBE} and E_c^{PBE} are the PBE exchange and correlation energy [57], respectively. There the suggestion for α is 0.25, focusing on atomization energies of a set of molecules. Here we follow a different rationale, and thus we perform a series of PBEh calculations for different values of α for the same molecule, and we use the Kohn-Sham eigenvalues and orbitals as input for subsequent G_0W_0 calculations. We find that $|\Delta_{\mathrm{HOMO}}^{\mathrm{qp}}|$ can be minimized by just a few single shot G_0W_0 calculations.

III. RESULTS AND DISCUSSION

In what follows, we present first our results for the TPA and OTAs obtained through different standard DFT functionals and HF, and we discuss the convergence of (mean-field) electronic properties with conjugation length. Next we analyze the G_0W_0@DFT and G_0W_0@HF results for differently sized OTAs, and we proceed to the discussion of the internally consistent procedure and the effects on the electronic structure in general.

A. Starting-point calculations

Our calculations are done for oligomers ranging from $n = 1$ (ethylene) to $n = 80$ double bonds OTA(80) and for the infinite TPA chain, over a single set of geometrical structures for all adopted functionals, so that we can evaluate the effect of each functional on the electronic properties independently from the effect on the structure (see Fig. 1). All calculations are performed using the FHI-AIMS code [58,59], which has the advantage of including all electrons, a feature of basic relevance in our case as we will use the core-level energies explicitly for

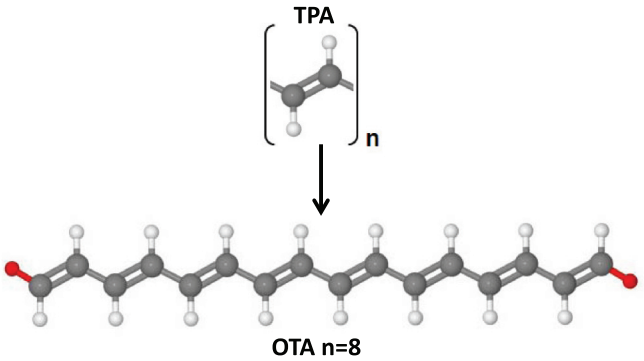

FIG. 1. (Color online) Schematic representation of the infinite polymer unit cell (TPA, top) and a finite model oligomer (OTA8, bottom), built by repetition of the unit cell. The hydrogen atoms added to saturate the oligomer chain and the resulting C-H distance are highlighted in red.

TABLE I. Ionization potential of acetylene oligomers, calculated at different theoretical levels: $-\epsilon_N$ negative of the KS (or HF) single-particle HOMO energy (left columns), our results for quasiparticle energies obtained through G_0W_0@DFT (right columns), scGW@HF, and from the internally consistent procedure; see the text (rightmost column). Experimental data are included for comparison at the center. All energies in eV. The mean absolute error for each functional as compared to the experimental values ($n = 1$–4) is included in the last row.

	DFT-KS		DFT-GKS				G_0W_0				scGW	
n	LDA	PBE	PBE0	B3LYP [78]	HF	Expt.	LDA	PBE	PBE0	HF	HF	icPBEh
1	6.85	6.66	7.77	7.26	10.10	10.51 [76]	10.20	10.25	10.36	10.70	10.02	10.44
2	5.95	5.75	6.68	6.23	8.60	9.07 [76]	8.65	8.62	8.83	9.25	8.47	8.97
3	5.51	5.31	6.13	5.69	7.82	8.29 [75]	7.78	7.74	8.00	8.48	7.65	8.18
4	5.26	5.04	5.80	5.36	7.33	7.79 [77]	7.20	7.17	7.47	8.01	7.15	7.69
5	5.09	4.87	5.57	5.14	7.01	7.00 [7][a]	6.84	6.80	7.10	7.69		7.36
6	4.97	4.75	5.41	4.97	6.78		6.56	6.50	6.81	7.46		7.12
8	4.59	4.81	5.19	4.75	6.48		6.17	6.09	6.44	7.16		6.79
MAE	3.03	3.23	2.32		0.45		0.46	0.47	0.25	0.19	0.59	0.10

[a]Experimental (gas-phase) data available only for polyenes with terminal *tert*-butyl groups; in this table, our calculated values for $n = 5$ are also for butyl-terminated molecules.

level alignment of different oligomers. Additionally, FHI-AIMS offers the possibility to calculate infinite periodic as well as finite systems with the same underlying approximations [60] (e.g., basis sets, integration grid). FHI-AIMS is written with numerical atomic-centered orbital basis sets, organized in so-called "*tiers*" of basis sets, providing excellent convergence of density-functional-based total energies even for complex structures, and sufficient convergence of G_0W_0 results [58,59]. For geometric structure determination, we use the high-accuracy *tier* 2 basis set (Table 1 of Ref. [58], 39 basis functions for C and 15 for H), and the calculations were carried out using the DFT functional of Perdew, Burke, and Ernzerhof [57] (PBE) augmented by the Tkatchenko and Scheffler van der Waals scheme (vdW$^{\rm TS}$) [61]. Unless otherwise stated, we select the *tier* 3 basis set (55 basis functions for C and 31 for H) to evaluate densities of states and quasiparticle energies. In the case of ΔSCF calculations, we work within the spin-restricted, i.e., non-spin-polarized approximation to evaluate the total energies for the ionized systems.

We first optimize the atomic coordinates for a TPA chain employing periodic boundary conditions, with the lattice constant along the chain direction fixed at the crystalline bulk value of $c = 2.457$ Å, as measured by x-ray scattering experiments [62]. To simulate a single isolated infinite-polymer chain, the polymer backbone is placed in the (x,z) plane (the converged ground-state geometry of the TPA is planar), and the lattice parameters perpendicular to the chain direction are set to a large value ($a = b = 25$ Å) in order to minimize the interaction between the chains in neighbor cells. A k-point mesh of $1 \times 1 \times 10$ is used in the optimization procedure. For these specific settings, the resulting carbon-carbon bond distances are 1.362 Å for the double bond (C=C) and 1.423 Å for the single bond (C−C), i.e., we obtain the expected dimerization of the polymer backbone. The C−H bond length is 1.095 Å and the C − C−C angle is found to be 123.8°. These structural parameters are quite similar to those found in previous theoretical studies using different functionals both within an oligomer approach [63] or solid-state calculations [64,65], and they also compare favorably with experimental results [66].

The DFT equilibrium structure of the isolated TPA chain is then used as input to build a series of linear oligomeric chains OTA(n). Since the focus of the present work is the length dependence of the electronic properties of oligomers, we keep the relative atomic coordinates fixed at the infinite chain result described above, and we perform a further optimization only for the C−H distance of the end-cap CH_2 groups. The details of the geometry are not our main focus, as long as the geometry is consistent. We thus keep the atomic coordinates of the PBE + vdW$^{\rm TS}$ optimization for each oligomer and apply different electronic structure approaches to these geometries. We first compare the following DFT functionals with HF: the local-density approximation as parametrized by Perdew and Zunger (LDA-PZ) [67,68], PBE, and PBE0 [52]. Then we perform G_0W_0 calculations on top of these DFT functionals and on top of HF. We also apply our internally consistent scheme. The calculations are performed for the finite oligomers with up to 30 double bonds ($n = 30$), which allows us to examine the length dependence of the frontier energy levels.

Discussing first the results obtained with the standard PBE functional, we show in Fig. 2 the KS energy-level spectra obtained for a selected series of oligomers and the density of states (DOS) for the infinite polymer chain. To align the levels of all systems, oligomers, and the TPA, we use the average of the core C_{1s} levels of each chain, which are then aligned at the value for the long oligomer OTA(50). As the chain length increases, we see the expected behavior of HOMO-LUMO gap closure, which converges to a small energy gap for the isolated TPA, in agreement with the literature results [34,69]. The main features of the continuum density of states of the polymer (i.e., the width of π HOMO and LUMO bands, and the position of localized π-states) start to be visible for chains with $\sim n = 15$ double bonds, in agreement with previous theoretical estimates [9].

B. IP of the transacetylene oligomer series

The scaling of physical properties of finite conjugated oligomers as a function of chain length has been extensively studied and modeled in experimental and theoretical works

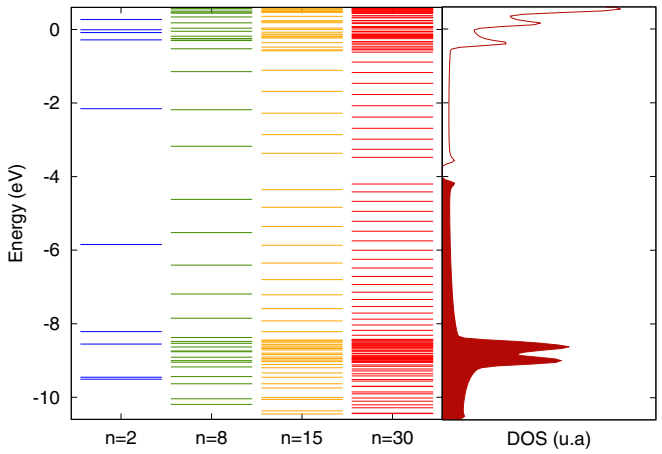

FIG. 2. (Color online) Discrete DFT energy level spectra (obtained with the PBE functional) of transacetylene oligomers (OTAs), compared to the density of states (DOS) of the 1D infinite polymer (TPA), calculated explicitly for the periodic model; here we use a Gaussian broadening of 0.05 eV for the DOS. Spectra aligned at the average of the core levels (C_{1s}) with those of OTA(50).

[9,10,12,70–74], aiming to predict the properties of polymeric materials using different extrapolation models. We thus move now to a comparison with experimental results, and in Table I we summarize the results for shorter oligomers, for which experimental data are available [7,75–77]. We first list the values coming directly from the negative of the HOMO eigenvalue (columns on the left) using the aforementioned different mean-field methods (KS and HF). Next we list the G_0W_0 results for the corresponding starting point, and finally the results from the internally consistent PBEh (columns on the right). We include also specific literature results obtained with the oft-employed hybrid functional B3LYP [78]. The experimental values are listed in the central column.

Considering first the comparison between experiment and the LDA and PBE eigenvalues ($-\epsilon_N^N$), we see that, as expected, the gas-phase IP of all oligomers is strongly underestimated. The agreement with experiment is only slightly improved by the hybrid functionals (PBE0 and B3LYP), while HF values are already very close.

In Figs. 3(a) and 3(b) we select PBE, PBE0, and HF and now consider the evolution of the IP obtained from the difference in total energies ($IP_{\Delta SCF}$). In Figs. 3(c) and 3(d), we directly compare the PBE HOMO eigenvalue with $IP_{\Delta SCF}$ for the PBE functional. We first note that $IP_{\Delta SCF}$ from HF and DFT differs by a few electronvolts for small- and medium-sized molecules, but also that this difference tends to increase with oligomer length. The $IP_{\Delta SCF}$ calculated with PBE (or PBE0) decreases quite fast with chain length. Indeed, we can see from Fig. 3 that the slope of DFT-$IP_{\Delta SCF}$ versus $1/l$ increases with chain length, thus the value of the IP does not stabilize at longer chain lengths. A different trend is seen for HF, that is, the $IP_{\Delta SCF}$ calculated with HF exhibits a decrease of the slope with growing oligomer length, a feature that can be seen more clearly following the inverse-length dependence. The fact that the slope in Fig. 3 increases for larger lengths in PBE and PBE0 must be attributed to the semilocal part and not to the nonlocal exchange part, because it does not happen for HF. The difference between the DFT and HF $IP_{\Delta SCF}$ reaches more than 1 eV in the infinite chain limit. We see also in Figs. 3(c) and 3(d) that the actual value of the negative of the PBE HOMO eigenvalue approaches the $IP_{\Delta SCF}$ at the infinite chain length limit, but the slopes of the two curves are quite different. We observe the same behavior for PBE0 (not shown here).

Let us now proceed to the quasiparticle picture: while KS-HOMO levels of organic molecules are usually too high for local or semilocal DFT functionals, many-body corrections introduced perturbatively via G_0W_0 calculations bring their values down, improving the description of IPs [31,79]. Our G_0W_0 results for the IPs in Table I illustrate that the differences in the quasiparticle energies are indeed significantly smaller than the differences in the HOMO energy for the original DFT or HF values. The corrected values are all in much better agreement with the measured values, with a mean absolute error smaller than 0.5 eV. However, contrary to the mean-field results, we now see an increasing deviation of the G_0W_0 IP from measured values with increasing oligomer length.

At this point, it is illuminating to also inspect the self-energy correction Δ^{qp}_{HOMO} to the KS HOMO level, as shown in Fig. 4 for PBE-based calculations. We observe that the self-energy correction decreases with chain length. This length dependence of Δ^{qp}_{HOMO} can be rationalized in terms of a length-dependent change in the screening strength of the oligomer. Given the specific π-character of the frontier orbitals, the electron density of the KS HOMO state delocalizes over the backbone of the oligomers, and when the molecular length is progressively increased from 0D ethylene toward quasi-1D oligomers, a substantial enhancement of the electronic screening is expected. The effect on the KS LUMO is similar for these systems, as we will see, and thus this is reflected in the value of the electronic gap. Niehaus *et al.* [80] report similar conclusions for the band gap of 1D polyacenes. Also for intrinsically different systems, sp^3-bonded silicon nanocrystals, Delerue and co-workers [81,82] observed in tight-binding GW calculations that the self-energy corrections to the DFT gap exhibit a smooth decreasing behavior with increasing (in that case 3D) nanocrystal size. These findings are in accordance with our results.

C. Internally consistent mixing parameter

We now move to the choice of the mixing parameter α to be inserted in the PBEh functional, Eq. (14). Figure 5 shows the results for G_0W_0 quasiparticle energies compared to the original PBEh(α) KS-HOMO energies for three chosen OTAs $n = 2$, 8, and 15. In this case, calculations are performed at the *tier* 2 basis-set level. As a consistency check, we compute the α^{ic} value for some selected oligomers using a larger basis set, namely *tier* 3, which allows for tightly converged orbital energies. The α^{ic} value is very stable with respect to the number of basis functions. Concerning the convergence behavior of both DFT eigenvalues and QP results, we observe that the energies of the highest occupied states shift down by $\lesssim$0.1 eV when going from *tier* 2 to *tier* 3 basis sets. These results indicate that *tier* 2 basis sets provide a good tradeoff between accuracy and computational cost for the systems we study here.

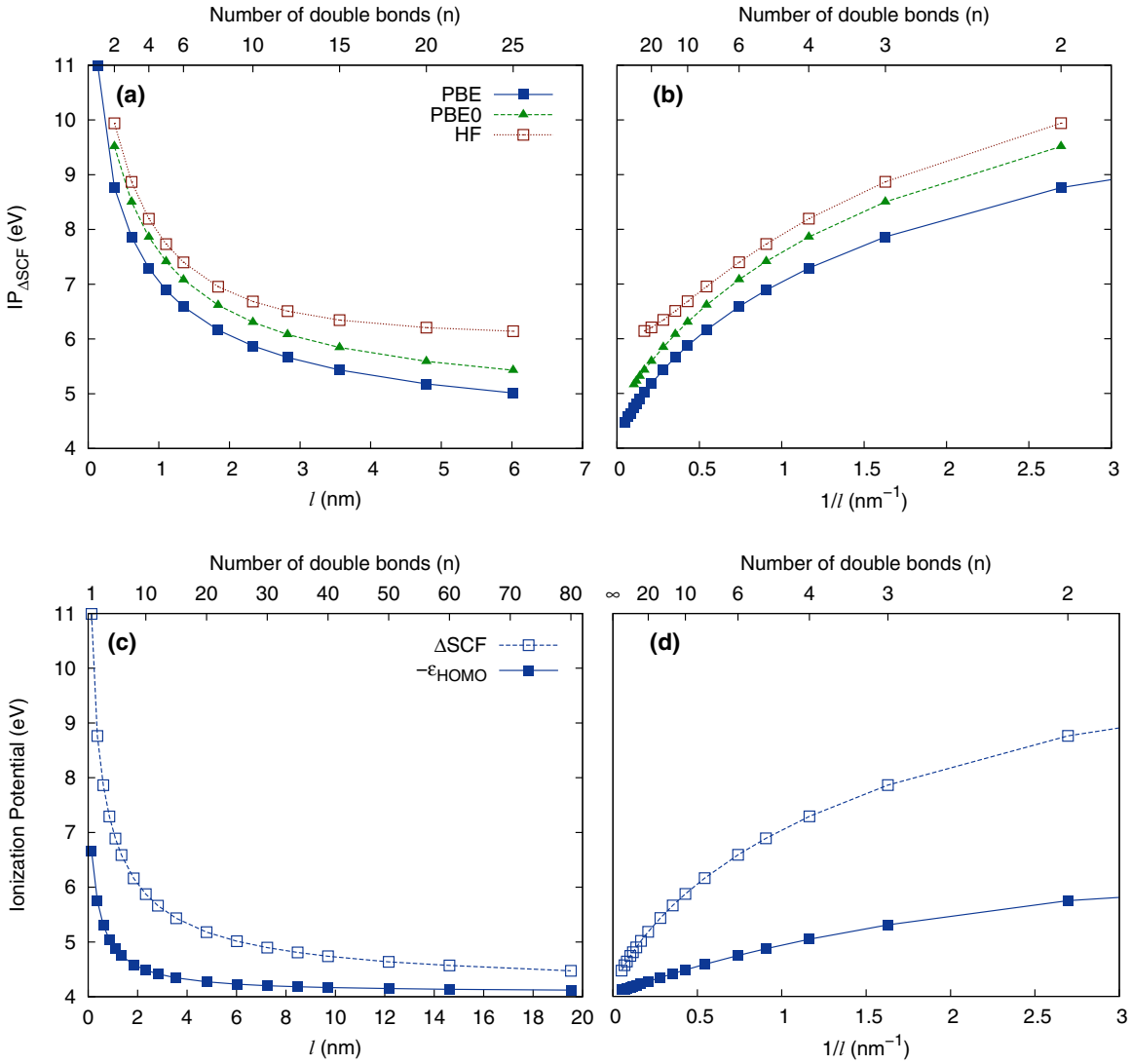

FIG. 3. (Color online) Top panel: Evolution of the first ionization potential of OTA series as a function of (a) chain length and (b) inverse chain length, up to $n = 30$ double bonds, calculated through the ΔSCF approach with the different methods PBE, PBE0, and HF. Bottom panel: Comparison of the negative HOMO energy and the ΔSCF approach obtained with the PBE functional, in the (c) chain length and (d) inverse chain length representation, up to $n = 80$ double bonds. The lines are just guides for the eye.

Figure 5 illustrates that the G_0W_0 HOMO energy depends less on the α parameter than the PBEh KS HOMO energy. The intersection between the PBEh and G_0W_0 curves defines the internally consistent fraction of EX, namely α^{ic}, and occurs at around $\alpha \simeq 0.8$. The α^{ic} for 1D conjugated oligomers is thus much higher than the fraction included in most standard hybrid functionals such as B3LYP (0.2), HSE, or PBE0 (0.25).

Our ic-PBEh IP values are also included in Table I (ic-PBEh) for $n = 1$–8. We see that we obtain an improved description of the highest occupied state, yielding IPs in good agreement with gas phase reference data, although no direct constraint is imposed in our scheme to fit experiment. Interestingly, the deviation of the ic-PBEh IPs from experiment remains approximately constant when increasing the oligomer length. This is shown in the inset of Fig. 6. We have also performed self-consistent GW (scGW) for reference, using the scGW implementation in FHI-AIMS [46,47]. The results are included in Table I. The scGW IPs are consistently lower than experiment, G_0W_0@PBE0 and ic-PBEh. This observation is consistent with recent benchmarks of scGW for molecules [43,46,47,83,84] and can be attributed to the pronounced deviation from the straight-line error (DSLE, also known as many-body self-interaction error) of scGW [84,85]. In G_0W_0, the DSLE can be reduced (or even eliminated) by an optimal starting point, which is why here we prefer to work with the ic-PBEh scheme.

We now point out that the starting-point dependence of G_0W_0 increases with system size, reaching ≈1.5 eV for $l \approx 7$ nm. This tells us that the G_0W_0 starting point is more important for longer or infinite chains. We thus plot in Fig. 7 our calculated α^{ic} as a function of system size. We note that it varies slightly with chain length, ranging from $\alpha \simeq 0.85$ for the ethylene molecule ($n = 1$) down to $\alpha \simeq 0.76$ for the longest chain with $n = 30$ double bonds. We fit $\alpha^{\text{ic}}(l)$ with an exponential, as indicated in Fig. 7, which allows us to estimate the consistent fraction of exact

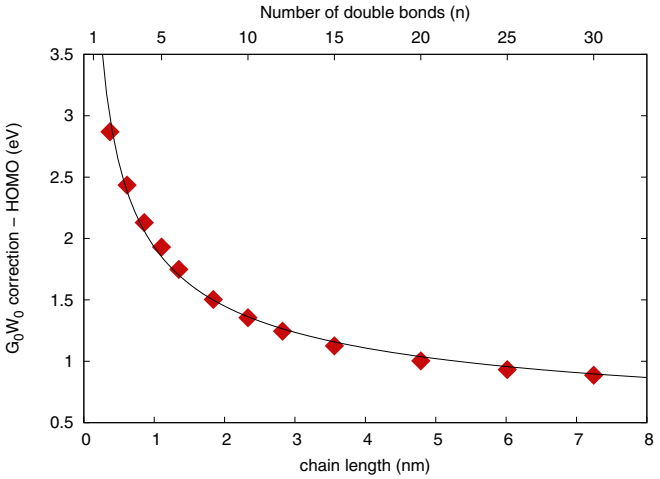

FIG. 4. (Color online) Length (l) dependence of the self-energy correction on the HOMO energy Δ^{qp}_{HOMO} of the OTA chains, defined as the difference between the quasiparticle and the KS energy; results for the PBE functional. The solid line is a fit with $\Delta^{qp}_{HOMO} = (1.6l^{-1/2} + 0.286)$ eV.

exchange in PBEh as 75% for the case of an isolated TPA chain [we also tested fitting with polynomials of $(1/l)$, but the errors are much larger]. In contrast, Körzdörfer *et al.* [86] recently studied long-range hybrid functionals with an additional range separation between the long-range Coulomb potential and a short-ranged effective density functional. They chose to optimize the range-separation parameter, not an overall exchange-mixing parameter α, finding that the range-separation parameter, optimized to satisfy the DFT analog of Koopmans' theorem, strongly depends on the chain length and does not exhibit a saturation behavior for long

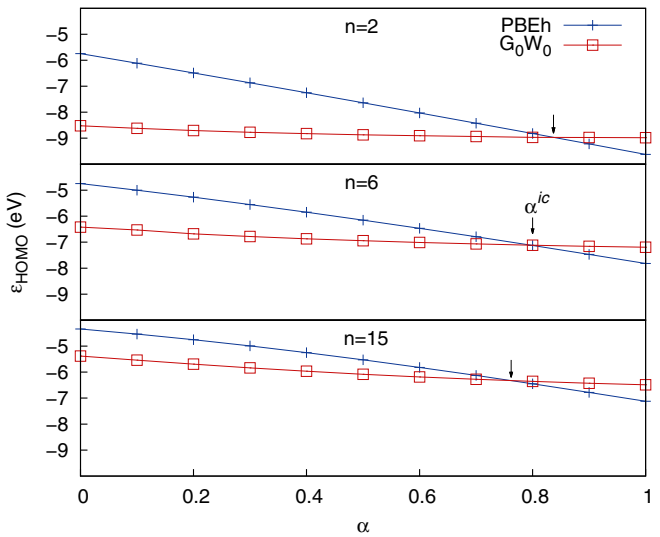

FIG. 5. (Color online) Evolution of the Kohn-Sham and quasiparticle HOMO energy of transacetylene oligomers with an increase of the mixing parameter α of PBEh. The parameter that satisfies the internal consistency criterion, α^{ic}, indicated in the central panel, corresponds to the crossing point between the curves calculated with PBEh(α) and G_0W_0@PBEh(α).

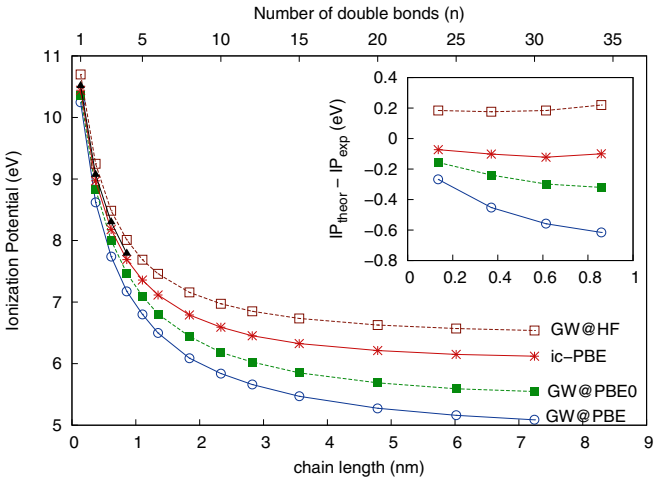

FIG. 6. (Color online) Chain length dependence of the first ionization potential of transacetylene oligomers obtained through G_0W_0 on different levels of mean-field methods: PBE (circles), PBE0 (solid squares), and internally consistent PBEh (stars); Hartree-Fock (empty squares). The lines are just guides for the eye. Included are also the experimental results (solid triangles) for small oligomers. Inset: difference between the calculated and experimental IP values for the small oligomers; same symbols as for the IP plots.

polyene chains ($n = 25$) regardless of the nature of the starting functional. Thus, tuning the exact exchange parameter α as proposed by the internally consistent scheme [50] is apparently a more adequate choice to predict the ionization potential for conjugated systems. As a last remark, we find that the optimal adjustment of the PBEh(α^{ic}) IP with length is obtained as $IP(l) = a + b/l + (ce^{-kl})/l$. A simpler inverse-length regression fails to reproduce the behavior at longer lengths, as already discussed for energy gaps [74,87,88].

Coming to more specific properties of these conjugated polymers, as pointed out before, the KS LUMO shows

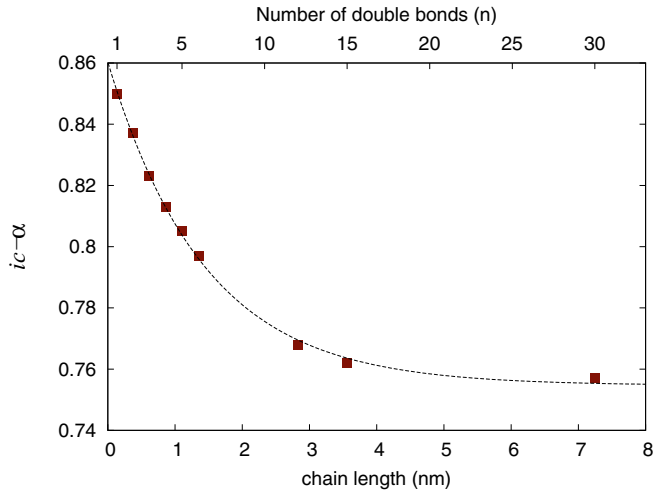

FIG. 7. (Color online) Size dependence of the internally consistent α-parameter of the PBEh functional obtained for transacetylene oligomers. We see that it decreases exponentially with chain length, as indicated by the dashed curve: the line is a fit with $\alpha^{ic}(l) = 0.106e^{-0.694l} + 0.755$.

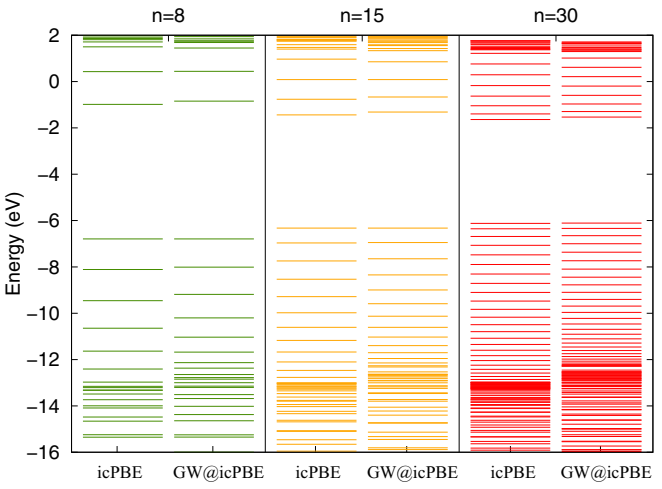

FIG. 8. (Color online) Comparison between the energy level spectra calculated at the PBEh(α^{ic}) and the G_0W_0@PBEh(α^{ic}) levels (with the internally consistent mixing parameter) for the $n = 8$, 15, and 30 acetylene oligomers, close to the HOMO-LUMO gap energy window.

π-conjugated symmetry and localization properties similar to the KS HOMO—as a consequence, we might expect that the behavior of the electronic gap also follows the same trend with tuning of α. We show in Fig. 8 the energy spectra obtained with our consistent procedure for intermediate length oligomers. We see that the HOMO-LUMO gaps obtained through PBEh(α^{ic}) are close to the quasiparticle G_0W_0 values.

We now extend our analysis to the eigenvalues for a large energy window, and not only the KS HOMO itself, and in Fig. 9 we include the results just for the PBE, i.e., PBEh($\alpha = 0$), and the PBEh(α^{ic}) starting points. In Fig. 9(a) we show the Δ_ϵ^{qp} energy corrections, for the same group of oligomers in Fig. 5, and in Fig. 9(b) we show the complete spectra coming from the different methods, for the longer chain $n = 30$ double bonds. Focusing on the eigenvalues close to the frontier orbitals, we first observe that the corrections to the first unoccupied PBEh(α^{ic}) states are really negligible, even for the $n = 15$ double-bond oligomer. Conversely, the corrections to the PBE eigenvalues are not only large ($\sim$1 eV) but also not constant as a function of energy. For the occupied states, the corrections to PBE are again large and not constant, but importantly they differ appreciably for localized and

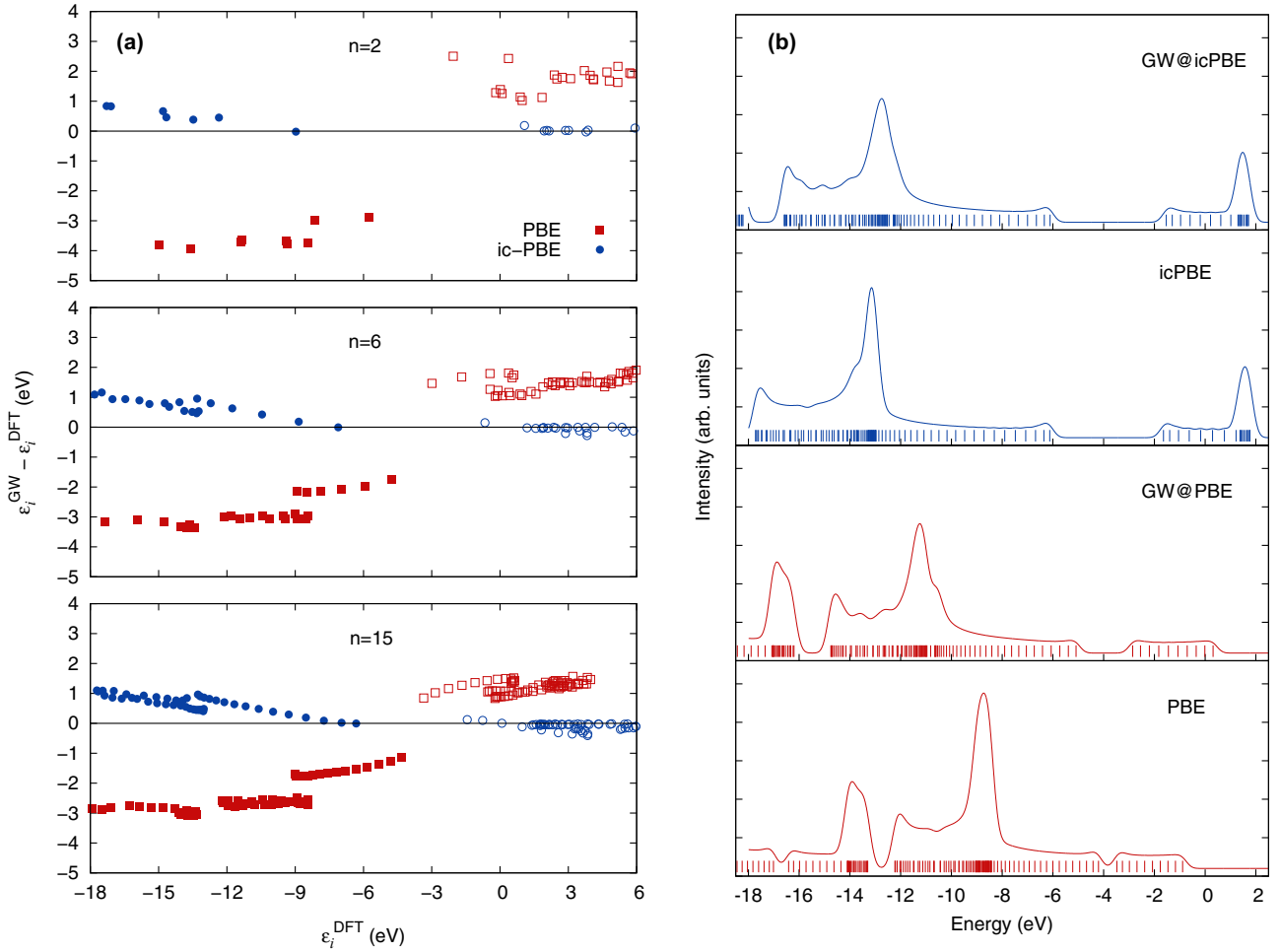

FIG. 9. (Color online) Comparison of PBEh(α^{ic}) (ic-PBE) with PBE: (a) Deviation of the Kohn-Sham (KS) eigenvalues with respect to the G_0W_0 quasiparticle spectrum plotted over the KS energies, for oligomer lengths $n = 2$, 6, and 15 double bonds. (b) Spectra obtained for the longer oligomer $n = 30$ double bonds by the different methodologies. In (a), filled symbols indicate occupied states, while empty symbols indicate unoccupied states.

delocalized states. We recall that the peak in the density of states at $\simeq$7 eV below the KS HOMO in Fig. 8 derives from localized states, thus from that energy down to the valence-band minimum we start to have mixing of states with different characteristics. The self-energy correction starting from PBE, for states in this energy window, is very different from the upper window values and is not predictable, while the correction to PBEh($\alpha^{\rm ic}$) follows a smooth trend and is always less than $\sim$1 eV; this is seen more clearly in Fig. 9(b). This analysis illustrates that PBEh($\alpha^{\rm ic}$) is a more suitable starting point for G_0W_0 than PBE, and thus it also indicates that the PBEh($\alpha^{\rm ic}$) spectrum is closer to experiment than PBE.

IV. SUMMARY AND CONCLUSIONS

In summary, we have presented and analyzed an "internally consistent" (ic) parametrization of the PBEh(α) functional that allows us to reproduce the electronic quasiparticle energies normally obtained from G_0W_0 calculations for the prototypical transacetylene family of conjugated systems. We show that the vertical ionization potential obtained with our optimized PBEh($\alpha^{\rm ic}$)functional, that is, obtained through a nonempirical constraint, is always in much better agreement with available experimental values than if a simpler semilocal or standard hybrid functional (B3LYP, PBE0) is used. Furthermore, our internally consistent scheme also yields good KS LUMO energies that are consistent with G_0W_0, although this consistency is not a requirement in the construction of the scheme. We thus also find good agreement for electronic gaps. As a last point, we show that many-body corrections to KS MO energies close to the frontier orbitals are also smaller than those obtained for standard functionals, which allows for a sound prediction of the valence photoemission spectra. The dependence of the optimal internally consistent exchange mixing parameter α on the chain length is discussed and found to converge with increasing chain length. This is a significant computational advantage, as the controlled behavior of the α parameter should allow one to perform a single ic parametrization step for a certain class of systems and then use the corresponding PBEh($\alpha^{\rm ic}$) functional for similar predictive simulations of the electronic structure of other, unknown systems of this class.

ACKNOWLEDGMENTS

The financial assistance of the Brazilian agencies CNPq and INCT-INEO is gratefully acknowledged. We also acknowledge the action of CAPES (Brazil) and DAAD (Germany) for financial support under Ph.D. grants. P.R. acknowledges the Academy of Finland through its Centres of Excellence Program (No. 251748).

[1] D. Cahen and A. Kahn, Adv. Mater. **15**, 271 (2003).
[2] A. P. Kulkarni, C. J. Tonzola, A. Babel, and S. A. Jenekhe, Chem. Mater. **16**, 4556 (2004).
[3] C.-G. Zhan, J. A. Nichols, and D. A. Dixon, J. Phys. Chem. A **107**, 4184 (2003).
[4] Y. Zhao, N. E. Schultz, and D. G. Truhlar, J. Chem. Theor. Comput. **2**, 364 (2006).
[5] G. Zhang and C. B. Musgrave, J. Phys. Chem. A **111**, 1554 (2007).
[6] I. Dabo, A. Ferretti, C.-H. Park, N. Poilvert, Y. Li, M. Cococcioni, and N. Marzari, Phys. Chem. Chem. Phys. **15**, 685 (2013).
[7] P. Rademacher, K. Kowski, H. Hopf, D. Klein, O. Klein, and C. Suhrada, J. Mol. Struct. **567-568**, 11 (2001).
[8] A. Ruini, M. J. Caldas, G. Bussi, and E. Molinari, Phys. Rev. Lett. **88**, 206403 (2002).
[9] G. R. Hutchison, Y.-J. Zhao, B. Delley, A. J. Freeman, M. A. Ratner, and T. J. Marks, Phys. Rev. B **68**, 035204 (2003).
[10] C. Chi and G. Wegner, Macromol. Rapid Commun. **26**, 1532 (2005).
[11] S. S. Zade, N. Zamoshchik, and M. Bendikov, Acc. Chem. Res. **44**, 14 (2011).
[12] W.-F. Li, M. Andrzejak, and H. A. Witek, Phys. Status Solidi B **249**, 306 (2012).
[13] A. Luzanov, J. Struct. Chem. **44**, 681 (2003).
[14] M. Musia and R. J. Bartlett, Chem. Phys. Lett. **384**, 210 (2004).
[15] M. Rohlfing, M. Tiago, and S. G. Louie, Synth. Met. **116**, 101 (2001).
[16] R. B. Capaz and M. J. Caldas, Phys. Rev. B **67**, 205205 (2003).
[17] A. Ferretti, A. Ruini, E. Molinari, and M. J. Caldas, Phys. Rev. Lett. **90**, 086401 (2003).
[18] M. Levy, J. P. Perdew, and V. Sahni, Phys. Rev. A **30**, 2745 (1984).
[19] C.-O. Almbladh and U. von Barth, Phys. Rev. B **31**, 3231 (1985).
[20] W. Yang, A. J. Cohen, and P. Mori-Sanchez, J. Chem. Phys. **136**, 204111 (2012).
[21] J. C. Slater, Adv. Quantum Chem. **6**, 1 (1972).
[22] D. A. Liberman, Phys. Rev. B **62**, 6851 (2000).
[23] J. A. Berger, P. L. de Boeij, and R. van Leeuwen, J. Chem. Phys. **123**, 174910 (2005).
[24] J. P. Perdew, R. G. Parr, M. Levy, and J. L. Balduz, Phys. Rev. Lett. **49**, 1691 (1982).
[25] U. Salzner and A. Aydin, J. Chem. Theor. Comput. **7**, 2568 (2011).
[26] L. Hedin, Phys. Rev. **139**, A796 (1965).
[27] L. Hedin and S. Lundqvist, Solid State Phys. **23**, 1 (1969).
[28] W. G. Aulbur, L. Jönsson, and J. W. Wilkins, Solid State Phys. **54**, 1 (2000).
[29] G. Onida, L. Reining, and A. Rubio, Rev. Mod. Phys. **74**, 601 (2002).
[30] P. Rinke, A. Qteish, J. Neugebauer, and M. Scheffler, Phys. Status Solidi B **245**, 929 (2008).
[31] X. Blase, C. Attaccalite, and V. Olevano, Phys. Rev. B **83**, 115103 (2011).
[32] C. Faber, I. Duchemin, T. Deutsch, C. Attaccalite, V. Olevano, and X. Blase, J. Mater. Sci. **47**, 7472 (2012).
[33] E. C. Ethridge, J. L. Fry, and M. Zaider, Phys. Rev. B **53**, 3662 (1996).
[34] M. Rohlfing and S. G. Louie, Phys. Rev. Lett. **82**, 1959 (1999).
[35] J.-W. van der Horst, P. A. Bobbert, M. A. J. Michels, G. Brocks, and P. J. Kelly, Phys. Rev. Lett. **83**, 4413 (1999).

[36] J.-W. van der Horst, P. A. Bobbert, P. H. L. de Jong, M. A. J. Michels, G. Brocks, and P. J. Kelly, Phys. Rev. B **61**, 15817 (2000).

[37] M. L. Tiago, M. Rohlfing, and S. G. Louie, Phys. Rev. B **70**, 193204 (2004).

[38] A. Ferretti, G. Mallia, L. Martin-Samos, G. Bussi, A. Ruini, B. Montanari, and N. M. Harrison, Phys. Rev. B **85**, 235105 (2012).

[39] Y.-W. Chang and B.-Y. Jin, J. Chem. Phys. **136**, 024110 (2012).

[40] F. Bruneval and M. A. L. Marques, J. Chem. Theor. Comput. **9**, 324 (2013).

[41] T. Körzdörfer and N. Marom, Phys. Rev. B **86**, 041110 (2012).

[42] T. Körzdörfer, R. M. Parrish, N. Marom, J. S. Sears, C. D. Sherrill, and J.-L. Brédas, Phys. Rev. B **86**, 205110 (2012).

[43] N. Marom, F. Caruso, X. Ren, O. T. Hofmann, T. Körzdörfer, J. R. Chelikowsky, A. Rubio, M. Scheffler, and P. Rinke, Phys. Rev. B **86**, 245127 (2012).

[44] P. Rinke, A. Qteish, J. Neugebauer, C. Freysoldt, and M. Scheffler, New. J. Phys. **7**, 126 (2005).

[45] F. Fuchs, J. Furthmüller, F. Bechstedt, M. Shishkin, and G. Kresse, Phys. Rev. B **76**, 115109 (2007).

[46] F. Caruso, P. Rinke, X. Ren, M. Scheffler, and A. Rubio, Phys. Rev. B **86**, 081102(R) (2012).

[47] F. Caruso, P. Rinke, X. Ren, A. Rubio, and M. Scheffler, Phys. Rev. B **88**, 075105 (2013).

[48] M. van Schilfgaarde, T. Kotani, and S. Faleev, Phys. Rev. Lett. **96**, 226402 (2006).

[49] A. Moliton and R. C. Hiorns, Polymer Int. **53**, 1397 (2004).

[50] V. Atalla, M. Yoon, F. Caruso, P. Rinke, and M. Scheffler, Phys. Rev. B **88**, 165122 (2013).

[51] N. A. Richter, S. Sicolo, S. V. Levchenko, J. Sauer, and M. Scheffler, Phys. Rev. Lett. **111**, 045502 (2013).

[52] J. P. Perdew, M. Ernzerhof, and K. Burke, J. Chem. Phys. **105**, 9982 (1996).

[53] C. Adamo and V. Barone, J. Chem. Phys. **110**, 6158 (1999).

[54] F. Bechstedt, *Many-Body Approach to Electronic Excitations*, Vol. 181 of Springer Series in Solid-State Sciences (Springer, Berlin, Heidelberg, 2015).

[55] M. M. Rieger, L. Steinbeck, I. White, H. Rojas, and R. Godby, Comput. Phys. Commun. **117**, 211 (1999).

[56] T. J. Pollehn, A. Schindlmayr, and R. W. Godby, J. Phys. Condens. Matter **10**, 1273 (1998).

[57] J. P. Perdew, K. Burke, and M. Ernzerhof, Phys. Rev. Lett. **77**, 3865 (1996).

[58] V. Blum, R. Gehrke, F. Hanke, P. Havu, V. Havu, X. Ren, K. Reuter, and M. Scheffler, Comput. Phys. Commun. **180**, 2175 (2009).

[59] X. Ren, P. Rinke, V. Blum, J. Wieferink, A. Tkatchenko, A. Sanfilippo, K. Reuter, and M. Scheffler, New. J. Phys. **14**, 053020 (2012).

[60] V. Havu, V. Blum, P. Havu, and M. Scheffler, J. Comp. Phys. **228**, 8367 (2009).

[61] A. Tkatchenko and M. Scheffler, Phys. Rev. Lett. **102**, 073005 (2009).

[62] C. R. Fincher, C. E. Chen, A. J. Heeger, A. G. MacDiarmid, and J. B. Hastings, Phys. Rev. Lett. **48**, 100 (1982).

[63] P. A. Limacher, K. V. Mikkelsen, and H. P. Lüthi, J. Chem. Phys. **130**, 194114 (2009).

[64] V. Lacivita, M. Reèrat, R. Orlando, M. Ferrero, and R. Dovesi, J. Chem. Phys. **136**, 114101 (2012).

[65] S. Hirata, H. Torii, and M. Tasumi, Phys. Rev. B **57**, 11994 (1998).

[66] C. S. Yannoni and T. C. Clarke, Phys. Rev. Lett. **51**, 1191 (1983).

[67] J. P. Perdew and A. Zunger, Phys. Rev. B **23**, 5048 (1981).

[68] D. M. Ceperley and B. J. Alder, Phys. Rev. Lett. **45**, 566 (1980).

[69] S. Rohra, E. Engel, and A. Görling, Phys. Rev. B **74**, 045119 (2006).

[70] S. Yang, P. Olishevski, and M. Kertesz, Synth. Met. **141**, 171 (2004).

[71] S. S. Zade and M. Bendikov, Org. Lett. **8**, 5243 (2006).

[72] J. Gierschner, J. Cornil, and H.-J. Egelhaaf, Adv. Mater. **19**, 173 (2007).

[73] M. J. G. Peach, E. I. Tellgren, P. Sałek, T. Helgaker, and D. J. Tozer, J. Phys. Chem. A **111**, 11930 (2007).

[74] J. Torras, J. Casanovas, and C. Alemán, J. Phys. Chem. A **116**, 7571 (2012).

[75] M. Beez, G. Bieri, H. Bock, and E. Heilbronner, Helv. Chim. Acta **56**, 1028 (1973).

[76] K. Kimura, *Handbook of HeI Photoelectron Spectra of Fundamental Organic Molecules: Ionization Energies, Ab Initio Assignments, and Valence Electronic Structure for 200 Molecules* (Halsted Press, New York; Japan Societies Press, Tokyo, 1981).

[77] T. Bally, S. Nitsche, K. Roth, and E. Haselbach, J. Am. Chem. Soc. **106**, 3927 (1984).

[78] U. Salzner, J. B. Lagowski, P. G. Pickup, and R. A. Poirier, J. Comput. Chem. **18**, 1943 (1997).

[79] C. Rostgaard, K. W. Jacobsen, and K. S. Thygesen, Phys. Rev. B **81**, 085103 (2010).

[80] T. A. Niehaus, M. Rohlfing, F. Della Sala, A. Di Carlo, and T. Frauenheim, Phys. Rev. A **71**, 022508 (2005).

[81] C. Delerue, M. Lannoo, and G. Allan, Phys. Rev. Lett. **84**, 2457 (2000).

[82] C. Delerue, G. Allan, and M. Lannoo, Phys. Rev. Lett. **90**, 076803 (2003).

[83] F. Caruso, V. Atalla, X. Ren, A. Rubio, M. Scheffler, and P. Rinke, Phys. Rev. B **90**, 085141 (2014).

[84] M. Hellgren, F. Caruso, D. R. Rohr, X. Ren, A. Rubio, M. Scheffler, and P. Rinke, Phys. Rev. B **91**, 165110 (2015).

[85] M. Dauth, F. Caruso, S. Kümmel, and P. Rinke (unpublished).

[86] T. Körzdörfer, J. S. Sears, C. Sutton, and J.-L. Brèdas, J. Chem. Phys. **135**, 204107 (2011).

[87] H. Meier, U. Stalmach, and H. Kolshorn, Acta Polym. **48**, 379 (1997).

[88] J. Rissler, Chem. Phys. Lett. **395**, 92 (2004).